

Julien BERGER

*Polytech Annecy-Chambéry, LOCIE, France*

Thomas BUSSER

*Polytech Annecy-Chambéry, LOCIE, France*

Denys DUTYKH

*CNRS-LAMA, Université Savoie Mont Blanc, France*

Nathan MENDES

*Pontifical Catholic University of Paraná, Brazil*

# ON THE ESTIMATION OF SORPTION ISOTHERM COEFFICIENTS USING THE OPTIMAL EXPERIMENT DESIGN APPROACH

LAST MODIFIED: October 14, 2019

# ON THE ESTIMATION OF SORPTION ISOTHERM COEFFICIENTS USING THE OPTIMAL EXPERIMENT DESIGN APPROACH

JULIEN BERGER\*, THOMAS BUSSER, DENYS DUTYKH, AND NATHAN MENDES

**ABSTRACT.** This paper deals with an inverse problem applied to the field of building physics to experimentally estimate three sorption isotherm coefficients of a wood fiber material. First, the mathematical model, based on convective transport of moisture, the optimal experiment design (OED) and the experimental set-up are presented. Then measurements of relative humidity within the material are carried out, after searching the OED, which is based on the computation of the sensitivity functions and *a priori* values of the unknown parameters employed in the mathematical model. The OED enables to plan the experimental conditions in terms of sensor positioning and boundary conditions out of 20 possible designs, ensuring the best accuracy for the identification method and, thus, for the estimated parameter. Two experimental procedures were identified: i) single step of relative humidity from 10 % to 75 % and ii) multiple steps of relative humidity 10 – 75 – 33 – 75 % with an 8-day duration period for each step. For both experiment designs, it has been shown that the sensor has to be placed near the impermeable boundary. After the measurements, the parameter estimation problem is solved using an interior point algorithm to minimize the cost function. Several tests are performed for the definition of the cost function, by using the  $\mathcal{L}_2$  or  $\mathcal{L}_\infty$  norm and considering the experiments separately or in the same time. It has been found out that the residual between the experimental data and the numerical model is minimized when considering the discrete Euclidean norm and both experiments separately. It means that two parameters are estimated using one experiment while the third parameter is determined with the other experiments. Two cost functions are defined and minimized for this approach. Moreover, the algorithm requires less than 100 computations of the direct model to obtain the solution. In addition, the OED sensitivity functions allow to capture an approximation of the probability distribution function of the estimated parameters. The determined sorption isotherm coefficients enable to calibrate the numerical model and fit better the experimental data, reducing the discrepancies usually reported in the literature that underestimate the moisture adsorption and overestimate the desorption processes.

**Key words and phrases:** Optimal Experiment Design (OED); parameter estimation problem; convective moisture transfer; sensitivity functions; sorption moisture coefficients

**MSC:** [2010] 35R30 (primary), 35K05, 80A20, 65M32 (secondary)

**PACS:** [2010] 44.05.+e (primary), 44.10.+i, 02.60.Cb, 02.70.Bf (secondary)

---

*Key words and phrases.* Optimal Experiment Design (OED); parameter estimation problem; convective moisture transfer; sensitivity functions; sorption moisture coefficients.

\* Corresponding author.

## CONTENTS

<b>1</b>	<b>Introduction</b>	<b>4</b>
1.1	Moisture transport in constructions	4
1.2	Inverse problems in building physics	5
1.3	Problem statement	7
<b>2</b>	<b>Methodology</b>	<b>7</b>
2.1	Physical problem	7
2.2	Dimensionless formulation	9
2.3	The Optimal Experiment Design	10
<b>3</b>	<b>Experimental facility</b>	<b>12</b>
<b>4</b>	<b>Searching the OED</b>	<b>15</b>
4.1	Estimation of one parameter	15
	Single step	15
	Multiple steps	15
4.2	Estimation of several parameters	16
	Single step	17
	Multiple steps	17
<b>5</b>	<b>Estimation of the unknown parameters</b>	<b>18</b>
5.1	Methodology	18
5.2	Results	22
<b>6</b>	<b>Final remarks</b>	<b>23</b>
6.1	Conclusion	23
6.2	Outlooks and open-problems	26
	Acknowledgments	26
	<b>References</b>	<b>28</b>

## 1. Introduction

Moisture in buildings has been a subject of major concern since the eighties. It may affect energy consumption and demand so we can mention at least four International Energy Agency projects conducted in the last 30 years to promote global research on this subject (Annexes 14, 24, 41 and 55) [1]. Furthermore, moisture can also have a dramatic impact on occupants' health and on material deterioration. Several tools have been developed to simulate the moisture transport in constructions as described in [54], which can be used to predict conduction loads associated to porous elements and mold growth risk in building enclosures. Nevertheless, those tools require input parameters containing temperature- and moisture- dependent hygrothermal properties.

### 1.1. Moisture transport in constructions

The following system of differential equations established by LUIKOV [39] represents the physical phenomenon of heat and mass transfer through capillary porous materials:

$$\frac{\partial U}{\partial t} = \nabla \cdot (a_m \nabla U + \delta a_m \nabla T), \quad (1.1a)$$

$$c_b \rho_0 \frac{\partial T}{\partial t} = \nabla \cdot (\lambda \nabla T) + r_{12} \nabla \cdot \left( a_{m1} \rho_0 (\nabla U + \delta_1 \nabla T) \right), \quad (1.1b)$$

where  $U$  is the relative concentration of moisture in the porous body,  $T$  the temperature,  $a_m$  the mass transfer coefficient for vapor (denoted with the subscript 1) and liquid inside the body,  $\delta$  the thermal-gradient coefficient,  $\rho_0$  the specific mass of the dry body,  $c_b$  the specific heat of the body and,  $r_{12}$  the latent heat of vaporization.

In building physics, those equations represent the physics that occurs in the building porous envelope and indoor porous elements such as furniture, textiles, *etc..* Regarding the envelope, the phenomenon is investigated to analyze the influence of moisture transfer on the total heat flux passing through the wall, with the objective of estimating the heat losses. They are also studied to analyze the durability of walls and to avoid disorders due to the presence of moisture as, for instance, mold growth, shrinking or interstitial condensation. This aspect is of major importance for wall configurations involving several materials with different properties, where moisture can be accumulated at the interface between two materials. Durability problems may also appear when considering important moisture sources as wind driven rain or rising damp problems. These analyses are performed by computing solutions to the partial differential equations. For this, numerical methods are used due to the nonlinearity of the material properties, depending on moisture content and temperature, and the non-stationary boundary conditions, defined as ROBIN-type and varying according to climatic data. Most of the numerical approaches consider standard discretization techniques. For the time discretisation, the EULER implicit [25, 42, 43] or explicit [34] schemes are adopted. Regarding the spatial discretisation, works in [40]

are based on finite-differences methods, in [5, 25, 41, 42] on finite-volume methods and in [30, 49] on finite-element methods. It is important to note that the solution of the equations requires the calculation of large systems of nonlinear equations (an order of  $10^6$  for 3-D problems). Furthermore, the problem deals with different time scales. The diffusive phenomena and the boundary conditions evolve on the time scale of seconds or minutes while the building performance usual analysis is done for a time interval of one year or even longer when dealing with durability or mold growth issues. Thus, the computation of heat and moisture transfer in porous material in building physics has a non-negligible computational cost. Recently, innovative and efficient methods of numerical simulation have been proposed. Some improved explicit schemes, enabling to overcome the stability restrictions of standard EULER explicit schemes, have been proposed in [26, 28]. An accurate and fast numerical scheme based on the SCHARFETTER–GUMMEL idea has been proposed in [12] to solve the advection-diffusion moisture differential equation. Some attempts based on model reduction methods, such as Proper Generalized Decomposition [9, 10, 13], Proper Orthogonal Decomposition [8, 40] and Spectral Reduced Order Models [27], have also been proposed.

## 1.2. Inverse problems in building physics

While some research focuses on numerical methods to compute the solution of the so-called direct problem to analyze the physical phenomena, some studies aim at solving inverse problems of heat and mass transfer in porous materials. In this case, the focus is the estimation of material properties  $(\gamma_0^\circ, c^\circ, a_m^\circ, \delta^\circ)$  using experimental data denoted as  $(T_{\text{exp}}, U_{\text{exp}})$  by minimizing a thoroughly chosen cost function  $J$ :

$$(\gamma_0^\circ, c^\circ, a_m^\circ, \delta^\circ) = \arg \min J,$$

$$\text{with } J = \left\| T_{\text{exp}} - T, U_{\text{exp}} - U \right\|,$$

where  $\left\| \dots \right\|$  is certain vector-norm.

Here, the inverse problem is an *inverse medium problem*, as it aims at estimating the coefficient of the main equation [31, 32]. Two contexts can be distinguished. First, when dealing with existing buildings to be retrofitted, samples cannot be extracted from the walls to determine their material properties. Therefore, some *in-situ* measurements are carried out according to a non-destructive design. The experimental data can be gathered by temperature, relative humidity, flux sensors and infrared thermography, among others. In most of the case, measurements are made at the boundary of the domain. From the obtained data, parameter estimation enables to determine the material thermo-physical properties. As mentioned before, the properties are moisture and temperature dependent. Therefore, the parameter identification problem needs to estimate functions that can be parameterized. Moreover, in such investigations, there is generally a few *a priori* information on the material properties. In [14], the thermal conductivity of an old historic building

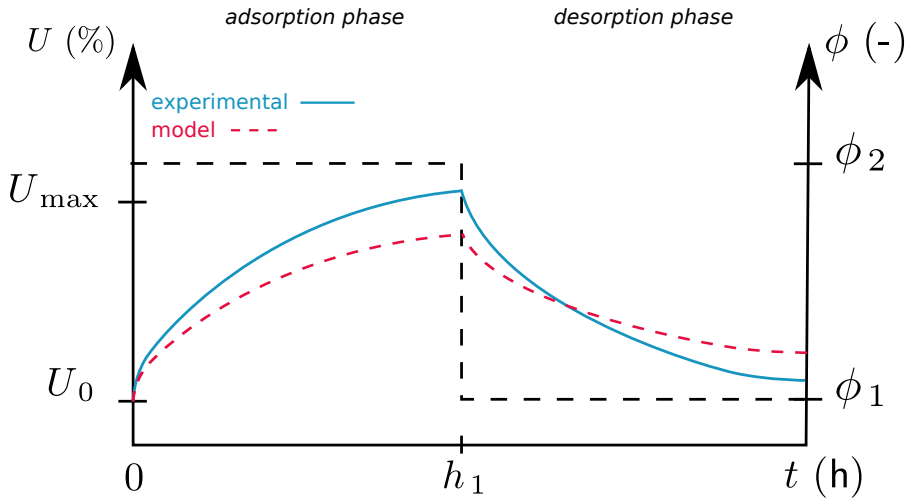


**Figure 1.** Illustration of the discrepancies observed when comparing experimental data to results from numerical model of moisture transfer in porous material.

wall composed of different materials is presented. In [50], the thermo-physical properties of materials composing a wall are estimated. In [44], the heat capacity and the thermal conductivity of a heterogeneous wall are determined. Once this parameter estimated, efficient simulations using the direct model can be performed to predict the wall conduction loads and at the end choose adequate retrofitting options.

Another issue arises when comparing the numerical model results and experimental data. Some discrepancies were observed as reported in several studies [12, 29] and illustrated in Figure 1. A material, with an initial moisture content  $U_0$ , is submitted to an adsorption and desorption cycles. Results from the simulation always underestimate the moisture adsorption process or overestimate the desorption process. To answer this issue, models can be calibrated using *in-situ* measurements for adapting the material properties to reduce the discrepancies between model predictions and real observations. In [35], moisture- and temperature-dependent diffusivity and thermo-physical properties are estimated using only temperature measurements under a drying process. In [9], the moisture permeability and advection coefficients are estimated using relative humidity measurements in a wood fiber material. In these cases, *a priori* information on the material properties are known thanks to complementary measurements based on well-established standards.

In terms of methodology for the estimation of parameters, several approaches can be distinguished in literature. Descent algorithms, based on the LEVENBERG–MARQUARDT algorithm, are used in [44]. Stochastic approaches, using BAYESIAN inferences and the MARKOV chain Monte Carlo algorithm, are applied in [14, 15, 21, 48]. Genetic algorithm based approaches are adopted to minimize the cost function in [18, 55]. Model reduction techniques, based on Proper Orthogonal Decomposition, are employed in [19].

### 1.3. Problem statement

This article presents the estimation of the moisture sorption isotherm coefficients of a wood fiber material, represented by three parameters, using an experimental facility, in order to reduce the discrepancies between model predictions and real performance. The estimation of the unknown parameters, based on observed data and identification methods, strongly depends on the experimental protocol. In particular, the boundary conditions imposed to the material and the location of sensors are of major importance. In [11], the concept of searching the Optimal Experiment Design (OED) was used to determine the best experimental conditions in terms of imposed flux and quantity and location of sensors, aiming at estimating the thermo-physical and hygrothermal properties of a material. The OED provides the best accuracy of the identification method and, thus, the estimated parameters.

Therefore, the main issue in this paper is to use the methodology to determine the OED considering the experimental set-up before starting the data acquisition. First, the optimal boundary conditions and location of sensors are defined. Then, the experimental campaign is carried out, respecting the OED. From the experimental data, the parameters are estimated using an interior-point algorithm with constraints on the unknowns. This article is organized as follows. Section 2 presents the physical problem with its mathematical formulation and the OED methodology. In Section 3, the existing experimental set up is described. The OED search providing the different possibilities for the estimation of one or several parameters with the experimental set up is presented in Section 4. The parameters are estimated in Section 5 and then the main conclusions are finally outlined.

## 2. Methodology

### 2.1. Physical problem

The physical problem involves unidimensional moisture convective transport through a porous material defined by the spatial domain  $\Omega_x = [0, L]$ . The moisture transfer occurs due to capillary migration, moisture diffusion and advection of the vapor phase. The physical problem represented by the convective moisture equation [7, 20, 39, 51]:

$$\frac{\partial \rho}{\partial t} = \frac{\partial}{\partial x} \left( d \frac{\partial P_v}{\partial x} \right) - \frac{\partial}{\partial x} \left( \frac{P_v}{R_v T} \mathbf{v} \right), \quad (2.1)$$

where  $\rho$  is the volumetric moisture content of the material,  $d$  the global moisture transport coefficient,  $P_v$  the vapor pressure,  $T$  the temperature,  $\mathbf{v}$  the mass average velocity and,  $R_v$  the water vapor gas constant. Eq. (2.1) is derived from Eq. (1.1a) by adding the moisture advection term. Moreover, the temperature remains the same at the boundaries. Even if heat transfer occurs in the material due to phase change, the temperature variations in the

material are assumed negligible. In addition, we can express the transient term as:

$$\frac{\partial \rho}{\partial t} = \frac{\partial \rho}{\partial \phi} \frac{\partial \phi}{\partial P_v} \frac{\partial P_v}{\partial t} + \frac{\partial \rho}{\partial T} \frac{\partial T}{\partial t}.$$

Under isothermal conditions, the second right-hand term of the equation above also vanishes. Considering the relation  $\rho = f(\phi) = f(P_v, T)$ , obtained from material properties and from the relation between the vapor pressure  $P_v$  and the relative humidity  $\phi$ , we get:

$$\frac{\partial \rho}{\partial t} = f'(P_v) \frac{1}{P_s} \frac{\partial P_v}{\partial t}.$$

For the advection term of Eq. (2.1), with the assumption of isothermal conditions and constant mass average velocity  $v$ , we can write:

$$\frac{\partial}{\partial x} \left( \frac{P_v}{R_v T} v \right) \simeq \frac{v}{R_v T} \frac{\partial P_v}{\partial x}.$$

Eq. (2.1) can be therefore rewritten as:

$$f'(P_v) \frac{1}{P_s} \frac{\partial P_v}{\partial t} = \frac{\partial}{\partial x} \left( d \frac{\partial P_v}{\partial x} \right) - \frac{v}{R_v T} \frac{\partial P_v}{\partial x}. \quad (2.2)$$

The material properties  $f'(P_v)$  and  $d$  depend on the vapor pressure  $P_v$ . We denote by:

$$c \stackrel{\text{def}}{=} \frac{f'(P_v)}{P_s}, \quad \text{the moisture storage coefficient}$$

$$a \stackrel{\text{def}}{=} \frac{v}{R_v T}, \quad \text{the global moisture advection coefficient}.$$

Therefore, the physical problem of convective moisture transport through a porous material can be mathematically described as:

$$c \frac{\partial P_v}{\partial t} = \frac{\partial}{\partial x} \left[ d \frac{\partial P_v}{\partial x} \right] - a \frac{\partial P_v}{\partial x}. \quad (2.3)$$

The moisture capacity  $c$  is assumed to be a second-degree polynomial of the relative humidity, while the moisture permeability  $d$  is considered as a first-degree polynomial of the relative humidity:

$$c = c_0 + c_1 \phi + c_2 \phi^2, \quad (2.4a)$$

$$d = d_0 + d_1 \phi. \quad (2.4b)$$

At  $x = 0$ , the surface is in contact with the ambient air at temperature  $T^\infty$  and relative humidity  $\phi^\infty$ . Thus, the boundary condition is expressed as:

$$d(\phi) \frac{\partial P_v}{\partial x} - a P_v = h \left( P_v - P_s(T^\infty) \phi^\infty(t) \right), \quad (2.5)$$

where  $h$  is the vapor convective transfer coefficient, considered as constant. At  $x = L$ , the surface is impermeable:

$$d \frac{\partial P_v}{\partial x} - a P_v = 0. \quad (2.6)$$

At  $t = 0$ , the vapor pressure is supposed to be uniform within the material

$$P_v = P_v^i. \quad (2.7)$$

## 2.2. Dimensionless formulation

For building porous material as concrete, insulation and brick, the coefficients scales with  $10^2$  for the sorption curve  $c$  and  $10^{-11}$  for the moisture permeability  $d$  and the advection coefficient  $a$ . Therefore, while performing a mathematical and numerical analysis of a given practical problem, it is of capital importance to obtain a unitless formulation of governing equations. For this, the vapor pressure is transformed to a dimensionless quantities:

$$u = \frac{P_v}{P_v^{\text{ref}}}, \quad u_i = \frac{P_v^i}{P_v^{\text{ref}}}, \quad u_\infty = \frac{P_s(T^\infty) \phi^\infty}{P_v^{\text{ref}}}.$$

The time and space domains are also modified:

$$x^* = \frac{x}{L}, \quad t^* = \frac{t}{t^{\text{ref}}},$$

where  $L$  is the length of the material and  $t^{\text{ref}}$  a characteristic time. The material properties are changed considering a reference value for each parameter:

$$c^* = \frac{c}{c_0}, \quad d^* = \frac{d}{d_0},$$

In this way, dimensionless numbers are highlighted:

$$\text{Pé} = \frac{a \cdot L}{d_0}, \quad \text{Bi} = \frac{h \cdot L}{d_0}, \quad \text{Fo} = \frac{t^{\text{ref}} \cdot d_0}{L^2 \cdot c_0}.$$

The dimensionless moisture BIOT number Bi quantifies the importance of the moisture transfer at the bounding surface of the material. The transient transfer mechanism is characterised by the FOURIER number Fo whereas the PÉCLET number Pé measures only the importance of moisture advection. The quantities  $c^*(u)$  and  $d^*(u)$  give the variation of storage and permeability coefficients from the reference state of the material. The dimensionless governing equations are finally written as:

$$c^*(u) \frac{\partial u}{\partial t^*} = \text{Fo} \frac{\partial}{\partial x^*} \left( d^*(u) \frac{\partial u}{\partial x^*} - \text{Pé} u \right), \quad t^* > 0, \quad x^* \in [0, 1], \quad (2.8a)$$

$$d^*(u) \frac{\partial u}{\partial x^*} - a^* u = \text{Bi} \cdot (u - u_\infty), \quad t^* > 0, \quad x^* = 0, \quad (2.8b)$$

$$d^*(u) \frac{\partial u}{\partial x^*} - a^* u = 0, \quad t^* > 0, \quad x^* = 1, \quad (2.8c)$$

$$u = u_i, \quad t^* = 0, \quad x^* \in [0, 1]. \quad (2.8d)$$

where functions  $c^*(u)$  and  $d^*(u)$  are given by:

$$\begin{aligned} c^*(u) &= 1 + c_1^* u + c_2^* u^2, \\ d^*(u) &= 1 + d_1^* u. \end{aligned}$$

The direct problem, defined by Eq. (2.8), is solved using a finite-difference standard discretisation method. An embedded adaptive in time RUNGE–KUTTA scheme combined with a SCHARFETTER–GUMMEL spatial discretisation approach, is used [12]. It is adaptive and embedded to estimate local error in time with low extra cost. The algorithm was implemented in the **Matlab** environment. For the sake of notation compactness, the upper-script  $\star$  standing for dimensionless parameters, is no longer used.

### 2.3. The Optimal Experiment Design

Efficient computational algorithms for recovering parameters  $\mathbf{P}$  given an observation  $u_{\text{exp}}$  of the field  $u(x, t)$  have already been proposed. Readers may refer to [46] for a primary overview of different methods. They are based on the minimization of the cost function  $J[\mathbf{P}]$ . For this purpose, it is required to equate to zero the derivatives of  $J[\mathbf{P}]$ , with respect to each of the unknown parameters  $p_m$  to find critical points. Associated to this necessary condition for the minimization of  $J[\mathbf{P}]$ , the scaled dimensionless local sensitivity function [24] is introduced:

$$\Theta_m(x, t) = \frac{\sigma_p}{\sigma_u} \frac{\partial u}{\partial p_m}, \quad \forall m \in \{1, \dots, M\}, \quad (2.9)$$

where  $\sigma_u$  is the variance of the error measuring  $u_{\text{exp}}$ . The parameter scaling factor  $\sigma_p$  equals to 1 as we consider that prior information on parameter  $p_m$  has low accuracy. It is important to note that all algorithms have been developed considering the dimensionless problem in order to compare only the order of variation of parameters and observation, avoiding the effects of units and scales.

The function  $\Theta_m$  measures the sensitivity of the estimated field  $u$  with respect to changes in the parameter  $p_m$  [4, 45, 46]. A small magnitude of  $\Theta_m$  indicates that large changes in  $p_m$  induce small changes in  $u$ . The estimation of parameter  $p_m$  is therefore difficult, in this case. When the sensitivity coefficient  $\Theta_m$  is small, the inverse problem is necessarily ill-conditioned. If the sensitivity coefficients are linearly dependent, the inverse problem is also ill-posed. Therefore, to get an optimal evaluation of parameters  $\mathbf{P}$ , it is desirable to have linearly-independent sensitivity functions  $\Theta_m$  with large magnitudes for all parameters  $p_m$ . These requirements ensure the best conditioning of the computational algorithm to solve the inverse problem and thus the better accuracy of the estimated parameter.

It is possible to define the experimental design in order to meet these requirements. The issue is to find the optimal sensor location  $X^\circ$  and the optimal amplitude  $\phi^{\infty, \circ}$  of the relative humidity of the ambient air at the material bounding surface,  $x = 0$ . To search

this optimal experiment design, we introduce the following measurement plan:

$$\pi \stackrel{\text{def}}{=} \{ X, \phi^\infty \}. \quad (2.10)$$

In the analysis of optimal experiments for estimating the unknown parameter(s)  $\mathbf{P}$ , a quality index describing the recovering accuracy is the  $D$ -optimum criterion [2, 3, 6, 22, 23, 53]:

$$\Psi = \det[F(\pi)], \quad (2.11)$$

where  $F(\pi)$  is the normalized FISHER information matrix [36, 52] defined as:

$$F(\pi) = [\Phi_{ij}], \quad \forall (i, j) \in \{1, \dots, M\}^2, \quad (2.12a)$$

$$\Phi_{ij} = \sum_{n=1}^N \int_0^\tau \Theta_i(x_n, t) \Theta_j(x_n, t) dt. \quad (2.12b)$$

The matrix  $F(\pi)$  characterizes the total sensitivity of the system as a function of the measurement plan  $\pi$  (Eq. (2.10)). The OED search aims at finding a measurement plan  $\pi^*$  for which the objective function (Eq. (2.11)) reaches the maximum value:

$$\pi^\circ = \{ X^\circ, \phi^{\infty, \circ} \} = \arg \max_{\pi} \Psi. \quad (2.13)$$

To solve Eq. (2.13), a domain of variation  $\Omega_\pi$  is considered for the sensor position  $X$  and the amplitude  $\phi^\infty$  of the boundary conditions. Then, the following steps are carried out for each value of the measurement plan  $\pi = \{ X, \phi^\infty \}$  in the domain  $\Omega_\pi$ . First, the direct problem, defined by Eqs. (2.3)-(2.7), is solved. Then, given the solution  $P_v$  for a fixed value of the measurement plan, the next step consists of computing the sensitivity coefficients  $\Theta_m = \frac{\partial u}{\partial p_m}$ , using also an embedded adaptive time RUNGE-KUTTA scheme combined with central spatial discretisation. Then, with the sensitivity coefficients, the FISHER matrix (2.12)(a,b) and the  $D$ -optimum criterion (2.11) are computed. The solution of the direct and sensitivity problems are obtained for a given *a priori* parameter  $\mathbf{P}$  and, in this case, the validity of the OED depends on this knowledge. If there is no prior information, the methodology of the OED can be done using an outer loop on the parameter  $\mathbf{P}$  sampled using, for instance, Latin hypercube or HALTON or SOBOL quasi-random samplings. Interested readers may refer to [11] for further details on the computation of sensitivity coefficients.

An interesting remark with this approach is that the probability distribution of the unknown parameter  $p_m$  can be estimated from the distribution of the measurements of the field  $u$  and from the sensitivity  $\Theta_m$ . The probability  $\mathcal{P}$  of  $u$  is given by:

$$F(\bar{u}) = \mathcal{P} \left\{ u(x, t, p_m) \leq \bar{u} \right\}.$$

Using the sensitivity function  $\Theta_m$ , the probability can be approximated by:

$$F(\bar{u}) \simeq \mathcal{P} \left\{ u(x, t, p_m^\circ) + \Theta_m \cdot (p_m - p_m^\circ) \leq \bar{u} \right\},$$

Assuming  $\Theta_m > 0$ , we get:

$$F(\bar{u}) = \mathcal{P} \left\{ p_m \leq p_m^\circ + \frac{\bar{u} - u(x, t, p_m^\circ)}{\Theta_m} \right\}.$$

Therefore, using a change of variable, the cumulative derivative function of the probability of the unknown parameter  $p_m$  is estimated by:

$$\begin{aligned} F(\bar{p}_m) &= \mathcal{P} \left\{ p_m \leq \bar{p}_m \right\}, \\ &= F \left( u + \Theta_m \cdot (\bar{p}_m - p_m^\circ) \right). \end{aligned}$$

When  $\Theta_m < 0$ , the cumulative derivative function of the probability is given by:

$$F(\bar{p}_m) = 1 - F \left( u + \Theta_m \cdot (\bar{p}_m - p_m^\circ) \right).$$

It gives a *local* approximation of the probability distribution of the unknown parameter  $p_m$ , at a reduced computational cost. Moreover, the approximation is reversible. Thus, if one has the distribution of the unknown parameter, it is possible to get the one of field  $u$ .

### 3. Experimental facility

The test facility used to carry out the experiment is illustrated in Figure 2. It is composed of two connected climatic chambers. The temperature of each chamber is controlled independently with a thermostatically-controlled water bath allowing water to recirculate in a heat exchanger. The relative humidity is kept fixed using saturated salt solutions of  $\text{MgCl}_2$  and  $\text{NaCl}$ . Relative humidity values in chambers 1 and 2 are fixed to  $\phi_1 = 33\%$  and  $\phi_2 = 75\%$ , respectively. Two door locks, at each side, allow the operator to insert or remove samples to minimize system disturbances. They enable easy and instantaneous change in humidity boundary conditions for the samples while passing from one chamber to another. Another climatic chamber is also available used to initially condition materials at  $\phi_0 = 10\%$ .

The temperature and relative humidity fields are measured within the samples with wireless sensors from the HygroPuce range (Waranet industry). The accuracy is  $\pm 2\%$  for the relative humidity and  $\pm 0.5^\circ\text{C}$  for the temperature and the dimensions are 0.6 cm thickness and 1.6 cm diameter, as illustrated in Figure 3(a). The sensors are placed within the material by cutting the samples. The total uncertainty on the measurement of relative humidity can be evaluated considering the propagation of the uncertainty due to sensor

Storage coefficient $c$	$c(u) = c_0 + c_1 u + c_2 u^2$
	$c_0 = 1, c_1 = -9.79 \cdot 10^{-1}, c_2 = 1.003$
Diffusion coefficient $d$	$d(u) = d_0 + d_1 u$
	$d_0 = 1, d_1 = 0.29$
PÉCLET number	$\text{Pé} = 1.1 \cdot 10^{-2}$
FOURIER number	$\text{Fo} = 4 \cdot 10^{-3}$
BIOT number	$\text{Bi} = 13.7$

**Table 1.** A priori dimensionless material properties of wood fiber from [9, 47].

measurement and due to their location. In [9] the total uncertainty on the measurement has been evaluated to  $\Delta\phi = 2\%$ .

The material investigated is the wood fibre, which properties have been determined in [9, 47] and are shown in its dimensionless form in Table 1. The reference parameter used to compute the unitless parameters are  $t^{\text{ref}} = 3600 \text{ s}$ ,  $d_0 = 5.17 \text{ s}$ ,  $c_0 = 2.85 \text{ kg}/(\text{m}^3 \cdot \text{Pa})$ ,  $L = 0.08 \text{ m}$  and  $P_v^{\text{ref}} = 1404 \text{ Pa}$ . It constitutes *a priori* information on the unknown parameters  $\text{Fo}$ ,  $c_1$  and  $c_2$ . The samples are cylindrical, with a 10 cm diameter and 8 cm thickness in order to avoid border effects and to minimize perturbations by sensors placed within the sample. Moreover, to ensure unidimensional moisture transfer and a null flux condition at  $x = 1$ , the samples are covered with aluminium tape and glued on a white acrylic seal, as illustrated in Figure 3(b). The convective moisture transport coefficient at  $x = 0$  has been estimated experimentally in [9, 16] following the protocol detailed in [38]. The corresponding BIOT number is reported in Table 1.

Finally, the experimental facility is used to submit the samples to a single or multiple steps of relative humidity. For a single step, the boundary conditions are defined as:

$$u_\infty(t) = \begin{cases} u_i, & t = 0, \\ u_c, & t > 0. \end{cases}$$

For the case of multiple steps, we set:

$$u_\infty(t) = \begin{cases} u_i, & t = 0 \\ u_c^1, & t \in (0, \tau], \\ u_c^2, & t \in (\tau, 2\tau], \\ u_c^3, & t \in (2\tau, 3\tau], \end{cases}$$

where the initial condition belongs to  $u_i \in \{0.2, 0.6, 1.5\}$ , the climatic chamber boundary condition  $(u_c, u_c^1, u_c^2, u_c^3) \in \{0.6, 1.5\}$  and the duration of the step  $\tau \in \{24, 48, 72, 96, 120, 144, 168, 192\}$ . A total of 20 designs are possible for providing measurements to estimate the unknown parameters  $\text{Fo}$ ,  $c_1$  and  $c_2$ .

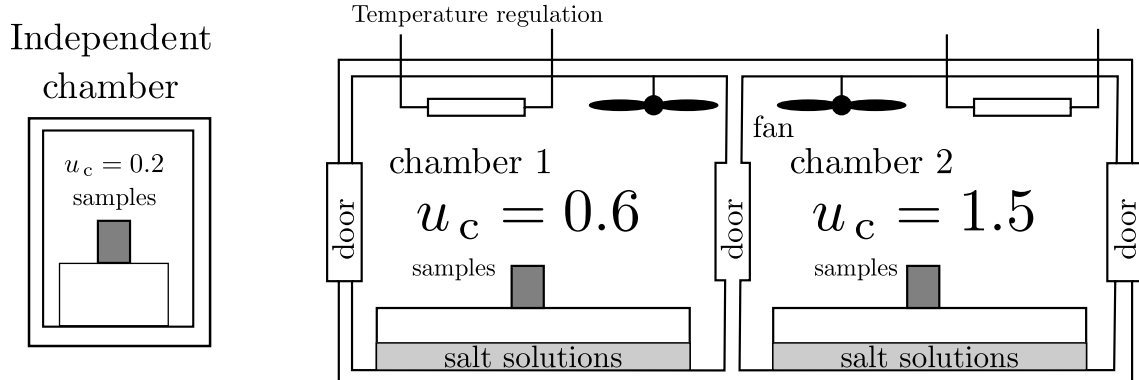


**Figure 2.** Illustration of the RH-box experimental facility.

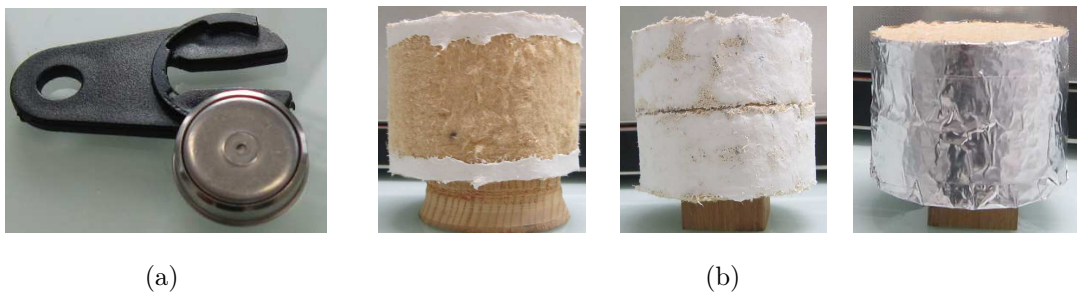


**Figure 3.** Sensors of relative humidity and temperature (a) and wood fibre samples (b) with white acrylic seal and with aluminium tape.

Single step			Multiple step							
			Case 1				Case 2			
Design	$u_i$	$u_c$	Design	$\tau$	Design	$\tau$	Design	$\tau$	Design	$\tau$
1	0.2	0.66	5	1	9	5	13	1	17	5
2	0.2	1.5	6	2	10	6	14	2	18	6
3	0.66	1.5	7	3	11	7	15	3	19	7
4	1.5	0.66	8	4	12	8	16	4	20	8

$$\text{Case 1: } u_i = 0.2, u_c^1 = 0.66, u_c^2 = 1.5, u_c^3 = 0.66$$

$$\text{Case 2: } u_i = 0.2, u_c^1 = 1.5, u_c^2 = 0.66, u_c^3 = 1.5$$

**Table 2.** Possible designs according to the experimental facility.

## 4. Searching the OED

### 4.1. Estimation of one parameter

This Section focuses on the estimation of one parameter within  $F_o$ ,  $c_1$  or  $c_2$  with experiments coming from single- or multiple-step designs. It should be noted that by estimating parameter  $F_o$ , the complete sorption isotherm curve is defined, according to the dimensionless quantities defined in Section 2.2.

#### 4.1.1 Single step

Figure 4(a) gives the variation of the criterion  $\Psi$  for the four single-step designs. For the estimation of parameters  $F_o$  or  $c_1$ , the criterion reaches its maximal value for design 2, corresponding to a step from  $u_i = 0.1$  to  $u_c = 1.5$ . For parameter  $c_2$ , the design 4 is the optimal one. It can be noted that, for parameter  $c_1$ , the relative criterion  $\Psi$  attains 80% for the design 4. It could be an interesting alternative to estimate this parameter. The variation of the criterion is related to the sensitivity function of each parameter. As noticed in Figures 5(a) and 5(b), functions  $\Theta$  have higher magnitudes of variation for the OED. The variation of  $\Psi$  as a function of the sensor location  $X$  is shown in Figure 4(b) for the OED. The optimal sensor location is at the boundary of the material opposite from the perturbations. If required for practical purpose, the sensor can be placed in the interval  $X \in [0.9, 1]$ , ensuring to reach 95% of the criterion  $\Psi$ . Results have similar tendencies for the three parameters.

#### 4.1.2 Multiple steps

Figure 6(a) shows the variation of the relative criterion  $\Psi$  for the designs considering multiple steps of relative humidity. It increases with the duration  $\tau$  of the steps. Thus, for the group of designs 5 to 12 and the group 13 to 20, the criteria reach their maximum for designs 12 and 20, respectively, corresponding to the step duration  $\tau = 8$ . The group 5 to 12 corresponds to a multiple step  $u_c^1 = 0.66$ ,  $u_c^2 = 1.5$ ,  $u_c^3 = 0.66$ . For them, the criterion does not attain 80% of the maximal criteria. Therefore, it is preferable to choose among designs 18 to 20, with a multiple step  $u_c^1 = 1.5$ ,  $u_c^2 = 0.66$ ,  $u_c^3 = 1.5$ , and a duration  $\tau \geq 6$  to estimate the parameters. Figures 7(a), 7(b) and 7(c) compare the sensitivity function of each parameter for three different designs. The quantity  $\Theta$  has higher magnitude of variation for the OED than for the others. Moreover, for the design 5, the duration of the step is so short that there is almost no variation in the sensitivity when occurring the first step for  $t \in [0, 24]$ . As for the previous case, the optimal sensor position is  $X \in [0.9, 1]$ .

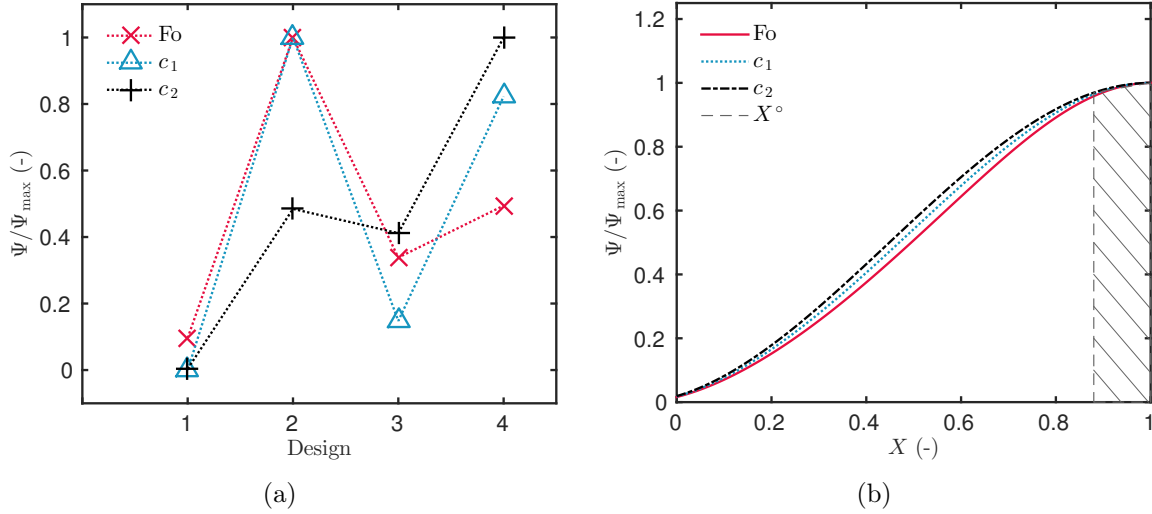


**Figure 4.** Variation of the criterion  $\Psi$  for the four possible single step designs (a) and as a function of the sensor position  $X$  for the OED (b), in the case of estimating one parameter.

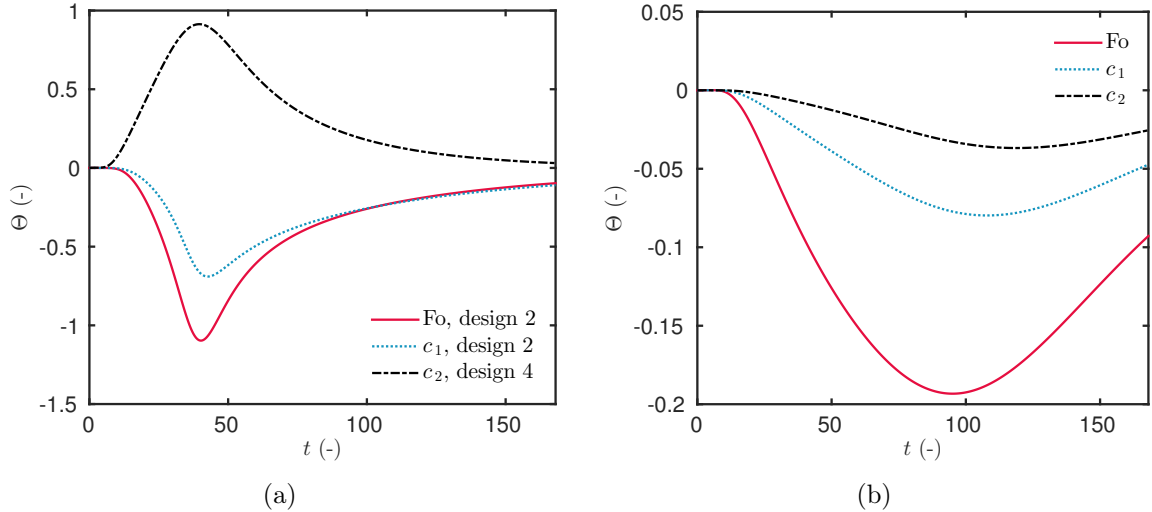


**Figure 5.** Sensitivity coefficients  $\Theta$  for parameters  $Fo$ ,  $c_1$  and  $c_2$  for the OED (a) and for design 1 (b) ( $X = X^\circ$ ).

## 4.2. Estimation of several parameters

The issue is now to estimate two or three parameters defining the moisture capacity  $Fo$ ,  $c_1$  and  $c_2$ . First of all, it is important to notice in Figures 5 and 7, that the sensitivity function  $\Theta$  of the parameters have a strong correlation. The interval of variation of the

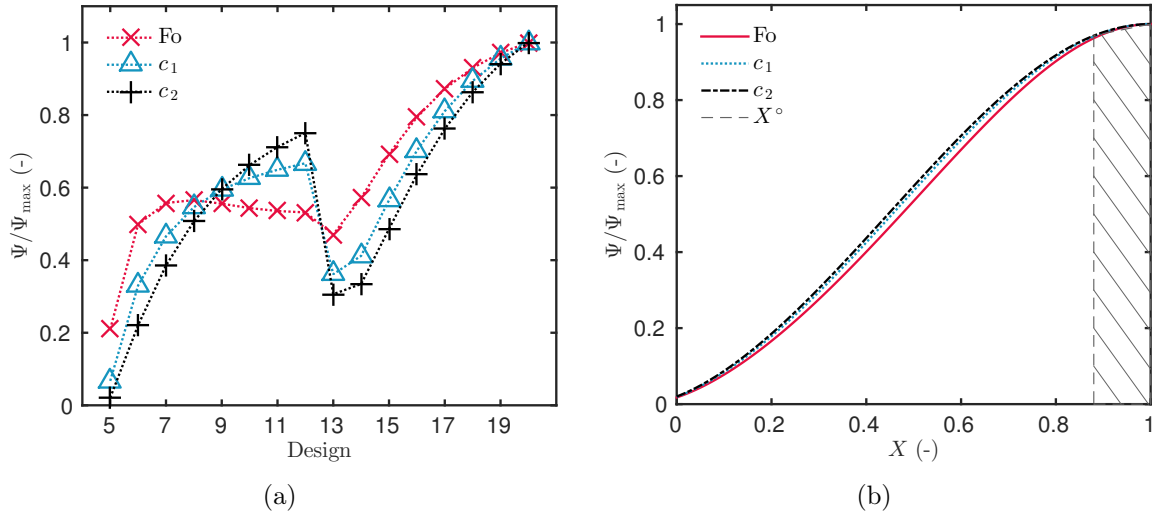


**Figure 6.** Variation of the criterion  $\Psi$  for the sixteen possible designs (a) and as a function of the sensor position  $X$  for the OED (b), in the case of estimating one parameter.

correlation coefficients for all the designs are:

$$\begin{aligned} r(Fo, c_1) &\in [0.94, 0.99], \\ r(c_1, c_2) &\in [0.92, 0.99], \\ r(Fo, c_2) &\in [0.71, 0.95]. \end{aligned}$$

Therefore, the estimation of the three parameters at the same time using only one experiment might be a difficult task. In addition, over all the possible designs, the couple of parameters  $(Fo, c_2)$  is the one with the lower correlation. Therefore, the OED search will only consider their estimation.

#### 4.2.1 Single step

Figure 8(a) gives the variation of the criterion  $\Psi$  for the four possible designs, considering a single step of relative humidity. The OED is reached for design 4. However, the design 2 represents an interesting alternative as more than 95% of the maximum criterion is reached. The sensor should be placed between  $X \in [0.9, 1]$ .

#### 4.2.2 Multiple steps

The variation of the criterion  $\Psi$  for the sixteen designs is shown in Figure 9. It increases with the duration of the steps  $\tau$ . The OED is reached for the design considering a multiple step  $u_i = 0.2$ ,  $u_c^1 = 1.5$ ,  $u_c^2 = 0.66$  and  $u_c^3 = 1.5$ , with a duration  $\tau = 8$ . As for the

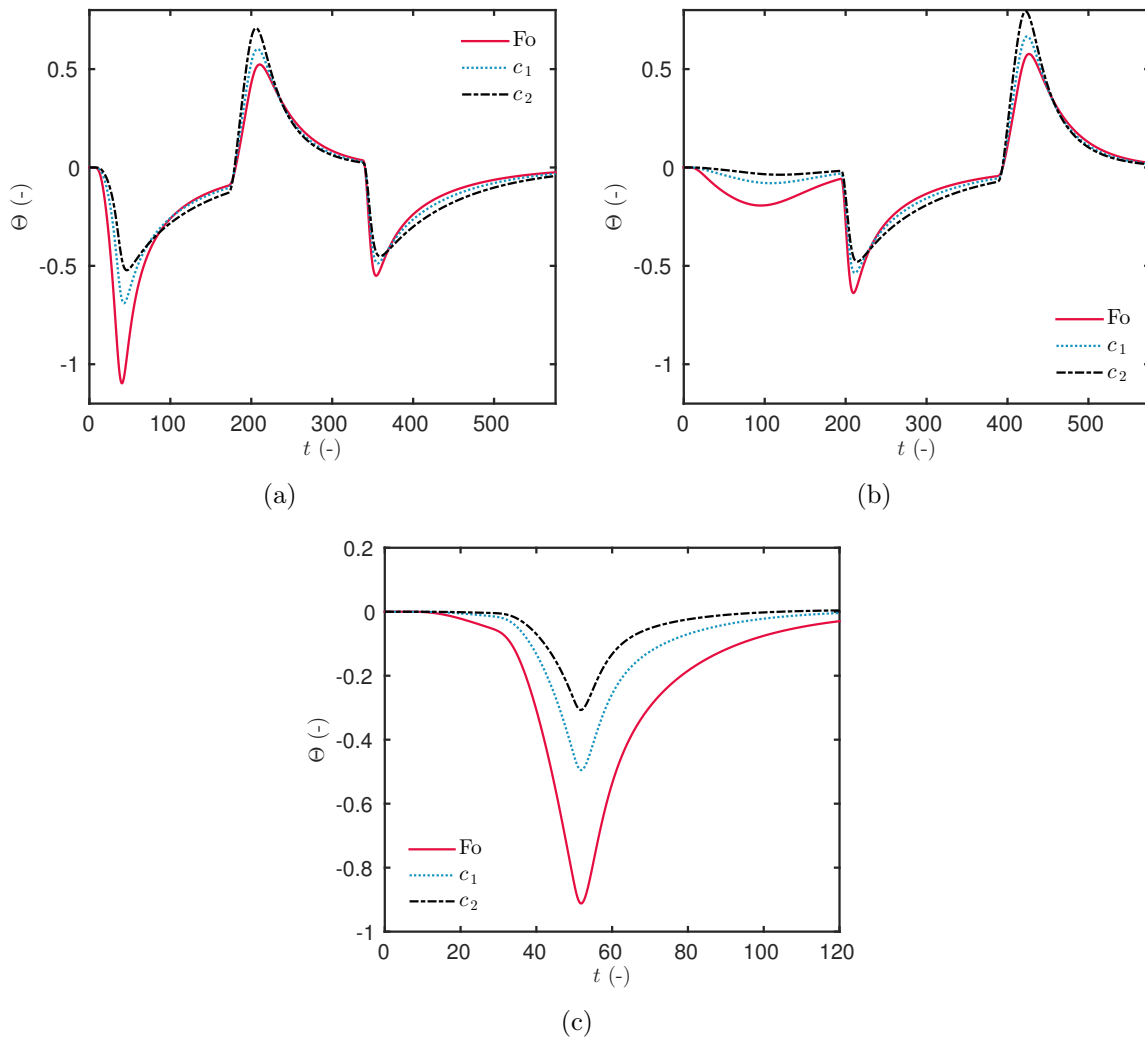


**Figure 7.** Sensitivity coefficients  $\Theta$  for parameters  $Fo$ ,  $c_1$  and  $c_2$  for the OED (design 20) (a), design 12 (b) and design 5 (c) ( $X = X^\circ$ ).

previous case, the OED is defined for a sensor placed near the boundary of the material  $x = 1$ .

## 5. Estimation of the unknown parameters

### 5.1. Methodology

As mentioned before, the sensitivity functions of parameters  $Fo$ ,  $c_1$  and  $c_2$  are strongly correlated and the estimation of the three parameters using one single experiment might be a laborious task. To answer this issue, a single step, referenced as experiment  $A$ , will be

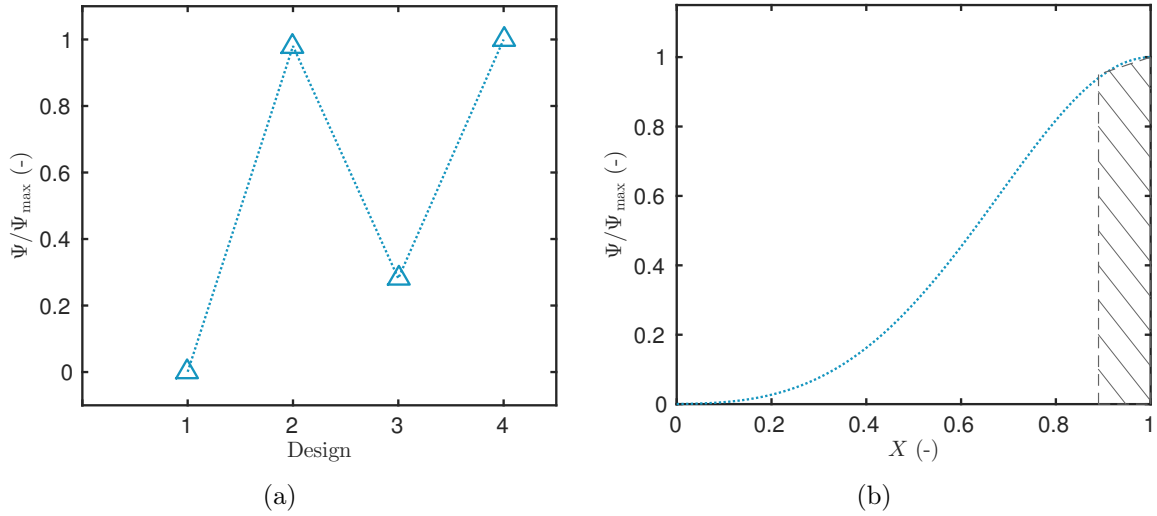


**Figure 8.** Variation of the criterion  $\Psi$  for the four possible designs of single step of relative humidity (a) and as a function of the sensor position  $X$  for the OED (b), in the case of estimating the couple of parameters  $(\text{Fo}, c_2)$ .

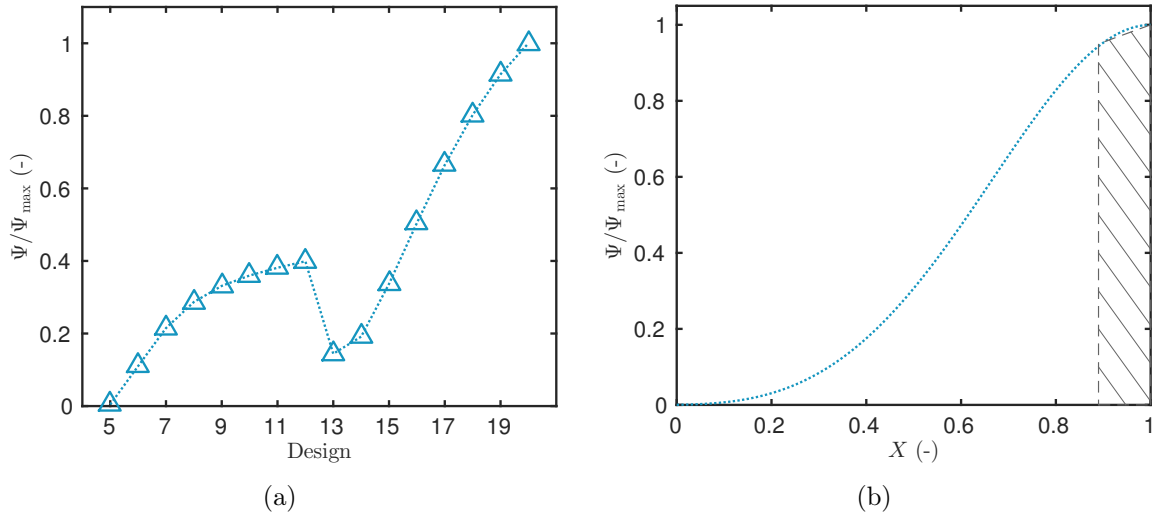


**Figure 9.** Variation of the criterion  $\Psi$  for the sixteen possible designs of multiple steps of relative humidity (a) and as a function of the sensor position  $X$  for the OED (b), in the case of estimating the couple of parameters  $(\text{Fo}, c_2)$ .

used for the estimation of the parameter  $c_1$  and a multiple step, referenced as experiment  $B$ , for the parameters  $(\text{Fo}, c_2)$ , which sensitivity functions are less correlated. According to the results of the OED, the sensor is placed near the border  $x = 1$ . For the boundary conditions, the single step will be operated from  $u_i = 0.2$  to  $u_c = 1.5$ . The OED multiple step is defined as  $u_i = 0.2$ ,  $u_c^1 = 1.5$ ,  $u_c^2 = 0.66$ ,  $u_c^3 = 1.5$  and a duration of each step  $\tau = 8$ .

To estimate the unknown parameters, the following cost function is defined by minimizing the residual between the experimental data and the numerical results of the direct model:

$$J_i^n = \left\| u - u_{\text{exp},n} \right\|_{\mathcal{L}_i}, \quad n \in \{1, 2, 3\}, \quad i \in \{2, \infty\}.$$

Several expressions of the cost function are tested. The subscript  $i$  denotes the norm used for the cost function  $J$ :  $i = 2$  stands for the standard discrete  $\mathcal{L}_2$  norm while  $i = \infty$  for the  $\mathcal{L}_\infty$  (uniform) norm.

The upper-script  $n = 1$  implies that both experiments are considered separately. The single step is used for estimating parameter  $c_1$  and the multiple step experiment for the parameters  $(\text{Fo}, c_2)$ . In such case, there is a cost function according to each experiment:

$$\begin{aligned} J_i^{1A}(\text{Fo}, c_2) &= \left\| u - u_{\text{exp},A} \right\|_{\mathcal{L}_i}, & \text{for the single step experiment} \\ J_i^{1B}(c_1) &= \left\| u - u_{\text{exp},B} \right\|_{\mathcal{L}_i}, & \text{for the multiple step experiment.} \end{aligned}$$

The estimation of the unknown parameters proceeds in an iterative approach as described in the algorithm 1. In this case, a tolerance  $\eta = 10^{-6}$  has been chosen.

```

1  $(\text{Fo}, c_1, c_2)^k = (\text{Fo}, c_1, c_2)^{\text{apr}}$  ;
2 while  $\|(\text{Fo}, c_1, c_2)^k - (\text{Fo}, c_1, c_2)^{k-1}\| \geq \eta$  do
3    $(\text{Fo}, c_2)^k = \arg \min J_i^{1A}$  ;
4    $(c_1)^k = \arg \min J_i^{1B}$  ;
5    $k = k + 1$  ;
6 end

```

**Algorithm 1:** *Estimation of the unknown parameters  $(\text{Fo}, c_1, c_2)$  considering both experiments separately with an iterative process.*

When  $n = \{2, 3\}$ , both experiments of single and multiple steps are considered at the same time, without any distinction. For  $n = 2$ , parameters  $(\text{Fo}, c_1, c_2)$  are estimated at once. An additional test, for  $n = 3$  is carried by considering both experiments to estimate all the material properties parameters  $(\text{Fo}, c_1, c_2, d_1, \text{Pé})$ . Thus, in these

cases, the cost functions are defined as:

$$\begin{aligned} J_2^2(Fo, c_1, c_2) &= \left\| u - u_{\text{exp},A} \right\|_{\mathcal{L}_2} + \left\| u - u_{\text{exp},B} \right\|_{\mathcal{L}_2}, \\ J_{\infty, \text{max}}^2(Fo, c_1, c_2) &= \max \left\{ \left\| u - u_{\text{exp},A} \right\|_{\mathcal{L}_{\infty}}, \left\| u - u_{\text{exp},B} \right\|_{\mathcal{L}_{\infty}} \right\}, \\ J_{\infty,+}^2(Fo, c_1, c_2) &= \left\| u - u_{\text{exp},A} \right\|_{\mathcal{L}_{\infty}} + \left\| u - u_{\text{exp},B} \right\|_{\mathcal{L}_{\infty}}, \end{aligned}$$

for  $n = 2$ , and for  $n = 3$ :

$$\begin{aligned} J_2^3(Fo, c_1, c_2, d_1, \text{Pé}) &= \left\| u - u_{\text{exp},A} \right\|_{\mathcal{L}_2} + \left\| u - u_{\text{exp},B} \right\|_{\mathcal{L}_2}, \\ J_{\infty, \text{max}}^3(Fo, c_1, c_2, d_1, \text{Pé}) &= \max \left\{ \left\| u - u_{\text{exp},A} \right\|_{\mathcal{L}_{\infty}}, \left\| u - u_{\text{exp},B} \right\|_{\mathcal{L}_{\infty}} \right\}, \\ J_{\infty,+}^3(Fo, c_1, c_2, d_1, \text{Pé}) &= \left\| u - u_{\text{exp},A} \right\|_{\mathcal{L}_{\infty}} + \left\| u - u_{\text{exp},B} \right\|_{\mathcal{L}_{\infty}}, \end{aligned}$$

Table 3 synthesizes all tests performed according to the definition of the cost function  $J$ . The cost function  $J$  is minimized using function `fmincon` in the Matlab environment, providing an efficient interior-point algorithm with constraint on the unknown parameters [17]. Here, the box-type constraints are defined with upper and lower bound for the parameters:

$$p^{\circ} \in [0.8, 1.5] \cdot p^{\text{apr}},$$

where the upper-scripts  $\circ$  and  $\text{apr}$  denote the estimated and *a priori* values of the parameters, respectively. The bounds have been defined by performing previous tests and analyzing the parameter impact on the calibration.

In order to quantify the quality of measured data, we estimate the noise inherent to any real physical measurement. By assuming that the noise  $\xi(\omega)$  is GAUSSIAN (*i.e.*  $\xi(\omega) \sim \mathcal{N}(0, \sigma^2)$ ), linear and additive, its variance  $\sigma^2$  can be thus estimated. Moreover, we assume that the underlying signal is smooth. In order to extract the noise component, the signal is approximated locally by a low-order polynomial representing the trend. Then, the trend is removed by using a special filter, leaving us with the pure noise content, which can be further analyzed using the standard statistical techniques. For the considered data, the variance equals:

$$\begin{aligned} \sigma &\simeq 0.01, & \text{for the single-step experiments,} \\ \sigma &\simeq 0.008, & \text{for the multiple-step experiments.} \end{aligned}$$

Definition of the cost function J	Tests								
	1	2	3	4	5	6	7	8	9
Experiments considered separately	x	x	x						
Experiments at the same time (3 parameters to estimate)				x	x	x			
Experiments at the same time (5 parameters to estimate)							x	x	x
Euclidean norm	x			x			x		
Infinite norm		x	x		x			x	
Sum of the infinite norms				x			x		x

**Table 3.** Synthesis of the tests carried out with the expression of the cost function.

The noise variance does not necessarily correspond to the measurement accuracy. This measure provides a lower bound of this error, *i.e.* the accuracy cannot be lower than the noise present in the measurement.

## 5.2. Results

Figure 10(a) shows the variation of the residual between the measured data and the numerical results for different tests performed. The residual is minimized for tests 1, 4 and 7, corresponding to the involving considering the EUCLIDEAN norm for the computation of the cost functions. The tendencies are similar for both experiments. It can be noted that the residual is lower when estimating only three parameters ( $Fo, c_1, c_2$ ) and not all the parameters of the material properties. Figure 10(b) provides the number of computations of the direct problem. As expected, the tests 1 to 3, considering both experiments separately, require a few more computations of the direct problem, due to the iterative procedure. Globally, the algorithm requires less than 100 computations, which is extremely low compared to stochastic approaches. For instance in [14],  $10^4$  computations are necessary to estimate the thermal conductivity of two materials by solving an inverse heat transfer problem.

The comparison of the measured data and numerical results is illustrated in Figure 11(a) for the one-step experiment. Figure 11(b) shows it for the multiple-step procedure, for the test 1. Results of the numerical model are provided for the *a priori* and estimated three parameters. As mentioned in the Introduction section, the numerical model with *a priori* parameters underestimates the moisture adsorption and overestimates the desorption processes. With the calibrated model, *i.e.* with the estimated parameters, there is a better agreement between the numerical results and the experimental data. Figures 11(c) and 11(d) show the residual. It is uncorrelated, highlighting a satisfactory estimation of the parameters. Nevertheless, it can be noted that some discrepancies remain between the experimental data and the numerical results. This can be specifically observed at  $t = 200$ ,

in Figures 11(b) and 11(d), for which some explanations are possible. First, the mathematical model may fail in representing the physical phenomenon. Some assumptions such as isothermal conditions, unidimensional transport and constant velocity might contribute to the differences observed between experimental and numerical results. Although the experiment has been conceived to be isothermal, slight variations in the temperature field occurs due to mechanisms of phase change that may affect the profile of vapor pressure, which is highly temperature dependent. On the other hand, despite the low relative humidity uncertainty, other uncertainties appear such as the interference of sensors on the moisture transfer through the sample, contact resistances and no perfect impermeabilization. Another possible explanation is associated to the parametrization of the material properties that can be improved. An interesting alternative could be to search for time varying parameters by adding a regularization term in the cost function  $J$ . The convergence of the parameter estimation is shown in Figure 12(a). On the contrary to parameters  $Fo$  and  $c_1$ , the *a priori* values of  $c_2$  is not far from the estimated one. After one iteration, the algorithm almost estimates the parameters. The number of computations of the direct model for test 1 is given in Figure 12(b). Only two global iterations are required to compute the solution of the inverse problem. More computations are required at the first iteration as the unknown parameters are more distant from the estimated optimal ones.

The computation of the sensitivity functions of the parameters to be estimated enables to approximate their probability density functions. The error is assumed as a normal distribution  $\mathcal{N}(0, \sigma_{\text{eff}}^2)$  with its standard deviation  $\sigma_{\text{eff}}$  computed by adding the ones due to uncertainty and to the noise:

$$\sigma_{\text{eff}} = \sigma_{\text{noise}} + \sigma_{\text{error}}.$$

Thus, the probability distribution is computed for different times as illustrated in Figure 13. As reported in Figure 7(a), the sensitivity function of parameters  $Fo$  and  $c_1$  is maximum and minimum at  $t = 207$  and  $t = 4$ , respectively. It explains why the probability function is maximum at  $t = 207$  for these parameters. Similar results can be observed when comparing the sensitivity function of parameter  $c_2$  in Figure 5(a) and the probability function in Figure 13(c).

## 6. Final remarks

### 6.1. Conclusion

In the context of building physics, inverse problems are encountered to estimate moisture dependent hygrothermal properties of porous materials, using measurements associated to heat and moisture transport. Two applications are distinguished. In the first case, concerning the diagnosis of existing building walls, there are few *a priori* estimations of the material properties. Moreover, measurements must be non-intrusive and non-destructive. In the second case, measurements are performed in the laboratory to calibrate the numerical

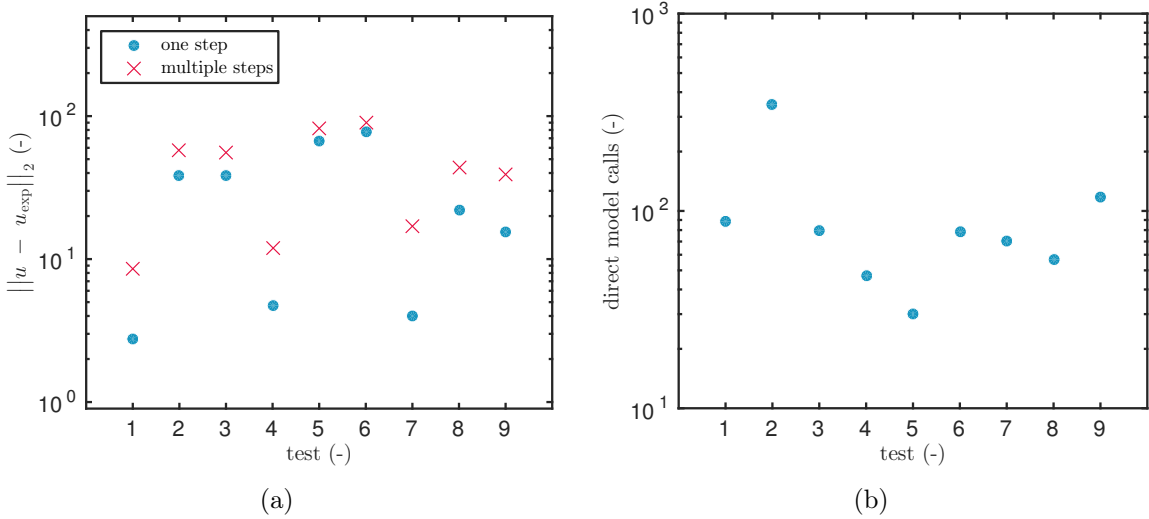


**Figure 10.** Residual between the measured data and numerical results for both experiments (a) and number of computations of the direct problem (b) for the different definition of the cost function  $J$ .

model with the experimental data. This article is encompassed in these conditions, focused on the estimation of three moisture sorption isotherm coefficients of a wood fiber material.

First, the OED methodology has been described and used for searching the optimal experiment design, ensuring to provide the best accuracy of the identification method for the parameter estimation. The approach is based on the sensitivity functions of the unknown parameters, enabling to determine sensor location within the material and boundary conditions, according to an existing facility among 20 possible designs. It has been carried out considering *a priori* values of the unknown parameters. The facility allows to submit material to relative humidity steps on one surface, being all others moisture impermeable. Results have enhanced two designs: i) single step of relative humidity from 10 % to 75 % and ii) multiple steps of relative humidity 10 – 75 – 33 – 75 %, with a duration period of 8 days for each step. For each design, the sensor has to be placed as close as possible to the impermeable boundary.

Then, experimental data have been provided according to the OED results for the two selected designs. The parameter estimation has been conducted by minimizing a cost function between the experimental data and the numerical results. The estimation has been accomplished using an interior point algorithm. Nine tests have been performed for the definition of the cost function  $J$ . The  $\mathcal{L}_2$  and  $\mathcal{L}_\infty$  have been evaluated. Two series of tests aimed at estimating the three parameters using both experiments at the same time or separately with an iterative algorithm. The third series intended to estimate all five parameters of the material properties. Results have shown that the  $\mathcal{L}_2$  norm provided better results of the parameter estimation problem. Moreover, it was better to consider both experiments separately to estimate only three parameters of the problem. Within this approach, the algorithm requires only two iterations to compute the solution with less

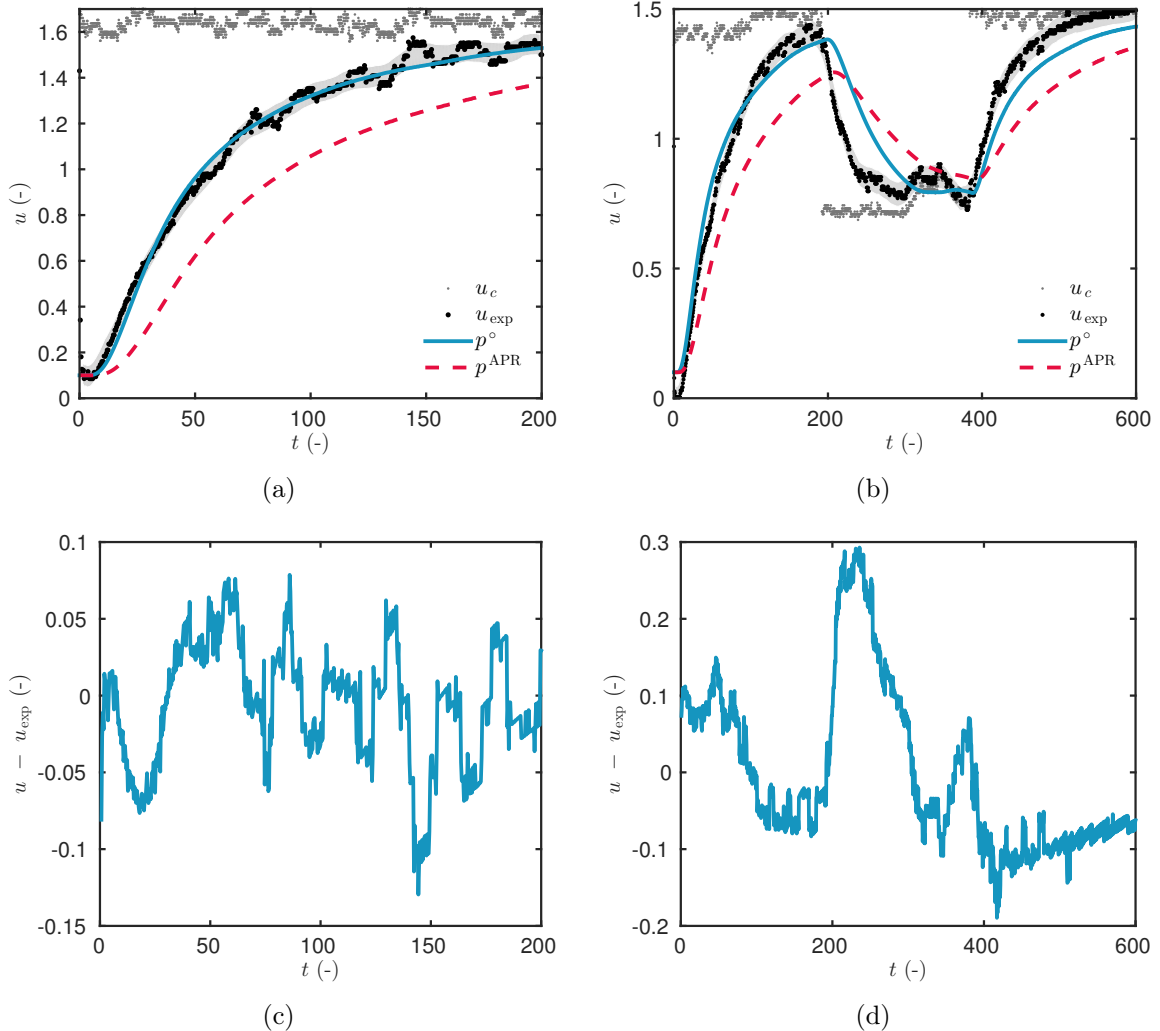


**Figure 11.** Comparison of the numerical results with the experimental data (a-b) and their 98% confidence interval for the single-step (a) and the multiple-step (b) experiments (test 1). Comparison of the residual for the single-step (c) and multiple-step (d) experiments.

than 100 computations of the direct model. This approach has a really low computational cost compared to stochastic approaches, needing an order of  $10^4$  computations for similar problems. Another advantage of this approach is to use the sensitivity function, computed during the search of the OED, to provide an approximation of the probability distribution function of the estimated parameters at a lower computational cost.

As highlighted in Section 5, the estimated parameter enables a better agreement of the numerical model with the experimental data. Particularly, the numerical results do not underestimate the moisture adsorption process or overestimate the desorption process, as usually reported in the literature [29]. The values of the estimated parameters are close to the *a priori* ones used for the search of the OED, validating the approach.

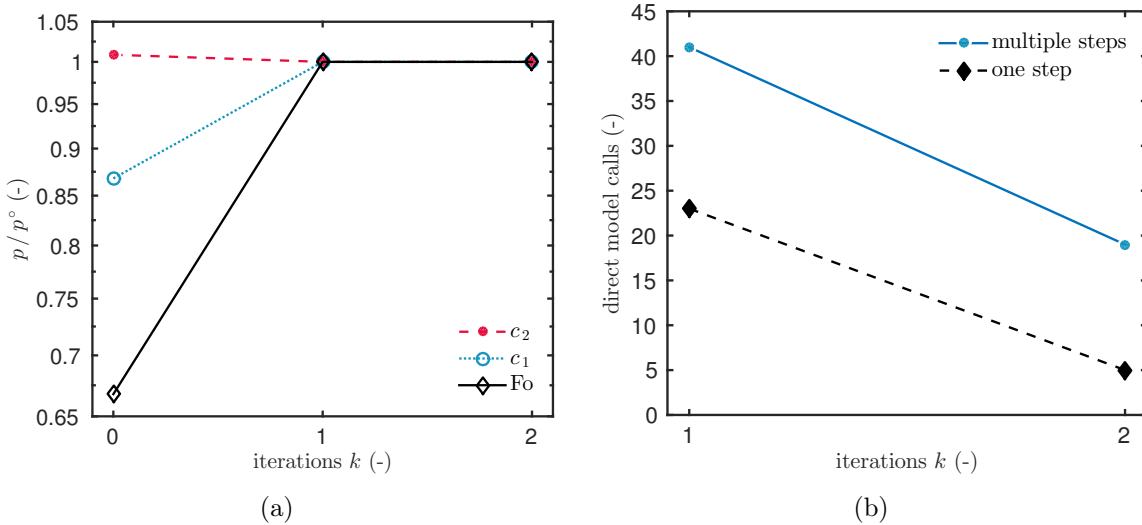


**Figure 12.** Convergence of the parameter estimation, for the test 1 as a function of the number of iterations (a) and number of computations of the direct model (b).

## 6.2. Outlooks and open-problems

As illustrated in Figure 11, some discrepancies still remain between the experimental data and the numerical calibrated model, which motivate further research to concentrate on improving the physical model by considering coupled heat and moisture transfer. Another interesting perspective of improvement concerns the assumptions related to the moisture sorption isotherm coefficients  $c(u)$ . A parametrization was previously defined  $c(u) = 1 + c_1 u + c_2 u^2$  and the parameter estimation problem aimed at identifying coefficients  $c_1, c_2$  (and  $Fo$ ). An ambitious outlook could aim at estimating directly the function  $c(u)$ , with inspiration from the following studies [33, 37].

## Acknowledgments

This work was partly funded by the French Environment and Energy Management Agency (ADEME), the “Assemblée des pays de Savoie” (APS) and the French National Research Agency (ANR) through its Sustainable Cities and Buildings program (MOBAIR project ANR-12-VBDU-0009).

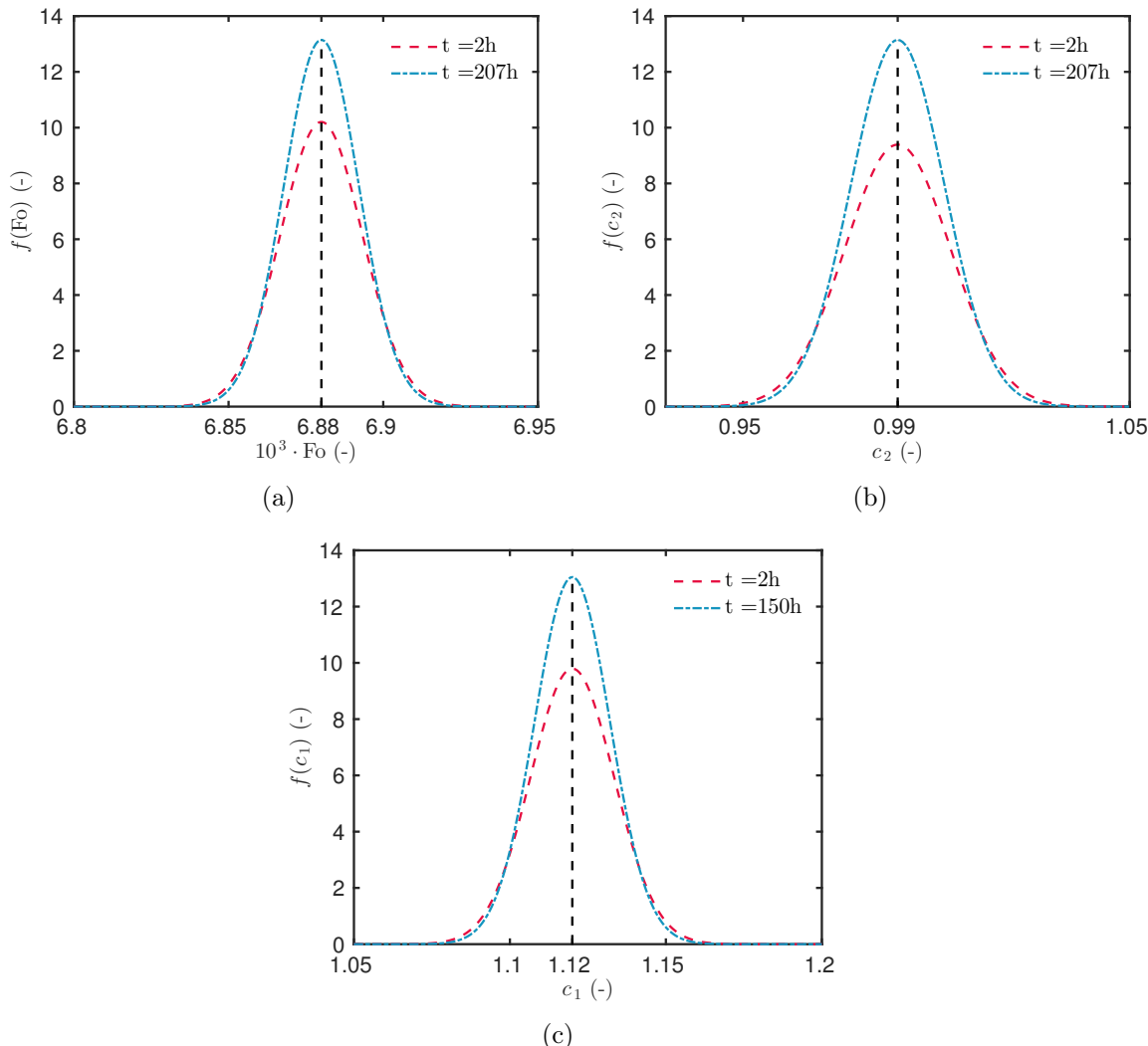


**Figure 13.** Probability density function approximated for the estimated parameters, computed using the sensitivity of single step (c) and a multiple step (a-b) experiments.

## Nomenclature

Latin letters		
$a$	moisture advection coefficient	[s/m]
$a_m$	mass transfer coefficient	[m <sup>2</sup> /s]
$c$	moisture storage capacity	[kg/(m <sup>3</sup> .Pa)]
$c_b$	specific heat	[J/(kg.K)]
$d$	moisture permeability	[s]
$h$	convective vapour transfer coefficient	[s/m]
$L$	length	[m]
$P_s$	saturation pressure	[Pa]
$P_v$	vapor pressure	[Pa]
$r_{12}$	latent heat of evaporation	[J/kg]
$R_v$	water gas constant	[J/(kg.K)]
$T$	temperature	[K]

Greek letters		
$\lambda$	thermal conductivity	[W/(m.K)]
$\delta$	thermal gradient coefficient	[K <sup>-1</sup> ]
$\phi$	relative humidity	[−]
$\rho$	specific mass	[kg/m <sup>3</sup> ]

## References

- [1] U. S. Energy Information Administration. *Annual Energy Outlook 2015, with projections to 2040*. EIA, Washington, DC, 2015. [4](#)
- [2] O. M. Alifanov, E. A. Artiukhine, and S. V. Rumyantsev. *Extreme Methods for Solving Ill-Posed Problems with Applications to Inverse Heat Transfer Problems*. Begellhouse, New York, 1995. [11](#)
- [3] M. L. Anderson, W. Bangerth, and G. F. Carey. Analysis of parameter sensitivity and experimental design for a class of nonlinear partial differential equations. *Int. J. Num. Meth. Fluids*, 48(6):583–605, jun 2005. [11](#)
- [4] E. A. Artyukhin and S. A. Budnik. Optimal planning of measurements in numerical experiment determination of the characteristics of a heat flux. *Journal of Engineering Physics*, 49(6):1453–1458, dec 1985. [10](#)
- [5] B. Bauklimatik Dresden. Simulation program for the calculation of coupled heat, moisture, air, pollutant, and salt transport. <http://www.bauklimatik-dresden.de/delphin/index.php?aLa=en>, 2011. [5](#)
- [6] J. V. Beck and K. J. Arnold. *Parameter Estimation in Engineering and Science*. John Wiley & Sons, Inc., New York, 1977. [11](#)
- [7] C. Belleudy, M. Woloszyn, M. Chhay, and M. Cosnier. A 2D model for coupled heat, air, and moisture transfer through porous media in contact with air channels. *Int. J. Heat Mass Transfer*, 95:453–465, apr 2016. [7](#)
- [8] J. Berger. *Contribution à la modélisation hygrothermique des bâtiments: Application des méthodes de réduction de modèle*. Phd thesis, Université de Grenoble, 2014. [5](#)
- [9] J. Berger, T. Busser, D. Dutykh, and N. Mendes. On the estimation of moisture permeability and advection coefficients of a wood fibre material using the optimal experiment design approach. *Submitted*, page 30, 2017. [5, 6, 13](#)
- [10] J. Berger, M. Chhay, S. Guernouti, and M. Woloszyn. Proper generalized decomposition for solving coupled heat and moisture transfer. *Journal of Building Performance Simulation*, 8(5):295–311, sep 2015. [5](#)
- [11] J. Berger, D. Dutykh, and N. Mendes. On the optimal experiment design for heat and moisture parameter estimation. *Exp. Therm. Fluid Sci.*, 81:109–122, feb 2017. [7, 11](#)
- [12] J. Berger, S. Gasparin, D. Dutykh, and N. Mendes. Accurate numerical simulation of moisture front in porous material. *Building and Environment*, 118:211–224, jun 2017. [5, 6, 10](#)
- [13] J. Berger, N. Mendes, S. Guernouti, M. Woloszyn, and F. Chinesta. Review of Reduced Order Models for Heat and Moisture Transfer in Building Physics with Emphasis in PGD Approaches. *Archives of Computational Methods in Engineering*, pages 1–13, jul 2016. [5](#)

- [14] J. Berger, H. R. B. Orlande, N. Mendes, and S. Guernouti. Bayesian inference for estimating thermal properties of a historic building wall. *Building and Environment*, 106:327–339, sep 2016. [5](#), [6](#), [22](#)
- [15] P. Biddulph, V. Gori, C. A. Elwell, C. Scott, C. Rye, R. Lowe, and T. Oreszczyn. Inferring the thermal resistance and effective thermal mass of a wall using frequent temperature and heat flux measurements. *Energy and Buildings*, 78:10–16, aug 2014. [6](#)
- [16] T. Bussler, A. Piot, M. Pailha, T. Bejat, and M. Woloszyn. From materials properties to modelling hygrothermal transfers of highly hygroscopic walls. In *CESBP*, Dresden, Germany, 2016. [13](#)
- [17] R. H. Byrd, J. C. Gilbert, and J. Nocedal. A Trust Region Method Based on Interior Point Techniques for Nonlinear Programming. *Math. Progr.*, 89(1):149–185, 2000. [21](#)
- [18] B. Czél and G. Gróf. Inverse identification of temperature-dependent thermal conductivity via genetic algorithm with cost function-based rearrangement of genes. *Int. J. Heat Mass Transfer*, 55(15-16):4254–4263, jul 2012. [6](#)
- [19] E. P. Del Barrio. Multidimensional inverse heat conduction problems solution via lagrange theory and model size reduction techniques. *Inverse Problems in Engineering*, 11(6):515–539, dec 2003. [6](#)
- [20] J. W. Delleur. *The handbook of groundwater engineering*. CRC Press, Boca Raton, FL, 2 edition, 2006. [7](#)
- [21] S. Dubois, F. McGregor, A. Evrard, A. Heath, and F. Lebeau. An inverse modelling approach to estimate the hygric parameters of clay-based masonry during a Moisture Buffer Value test. *Building and Environment*, 81:192–203, nov 2014. [6](#)
- [22] A. F. Emery and A. V. Nenarokomov. Optimal experiment design. *Measurement Science and Technology*, 9(6):864–876, jun 1998. [11](#)
- [23] T. D. Fadale, A. V. Nenarokomov, and A. F. Emery. Two Approaches to Optimal Sensor Locations. *Journal of Heat Transfer*, 117(2):373, 1995. [11](#)
- [24] S. Finsterle. Practical notes on local data-worth analysis. *Water Resources Research*, 51(12):9904–9924, dec 2015. [10](#)
- [25] I. Fraunhofer. Wufi. [http://www.hoki.ibp.fhg.de/wufi/wufi\\_frame\\_e.html](http://www.hoki.ibp.fhg.de/wufi/wufi_frame_e.html), 2005. [4](#), [5](#)
- [26] S. Gasparin, J. Berger, D. Dutykh, and N. Mendes. An improved explicit scheme for whole-building hygrothermal simulation. *Submitted*, page 40, 2017. [5](#)
- [27] S. Gasparin, J. Berger, D. Dutykh, and N. Mendes. Spectral reduced order model for predicting nonlinear moisture transfer in hygroscopic materials. *Submitted*, page 30, 2017. [5](#)
- [28] S. Gasparin, J. Berger, D. Dutykh, and N. Mendes. Stable explicit schemes for simulation of nonlinear moisture transfer in porous materials. *J. Building Perf. Simul.*, pages 1–21, 2017. [5](#)
- [29] C. James, C. J. Simonson, P. Talukdar, and S. Roels. Numerical and experimental data set for benchmarking hygroscopic buffering models. *Int. J. Heat Mass Transfer*, 53(19-20):3638–3654, sep 2010. [6](#), [25](#)
- [30] H. Janssen, B. Blocken, and J. Carmeliet. Conservative modelling of the moisture and heat transfer in building components under atmospheric excitation. *Int. J. Heat Mass Transfer*, 50(5-6):1128–1140, mar 2007. [5](#)
- [31] S. I. Kabanikhin. Definitions and examples of inverse and ill-posed problems. *J. Inv. Ill-posed Problems*, 16(4):317–357, jan 2008. [5](#)
- [32] S. I. Kabanikhin. *Inverse and ill-posed problems: theory and applications*. Walter De Gruyter, Berlin, 2011. [5](#)

[33] S. I. Kabanikhin, A. Hasanov, and A. V. Penenko. A gradient descent method for solving an inverse coefficient heat conduction problem. *Numerical Analysis and Applications*, 1(1):34–45, jan 2008. [26](#)

[34] A. S. Kalagiris, P. Weitzmann, T. R. Nielsen, R. Peuhkuri, C.-E. Hagentoft, and C. Rode. The International Building Physics Toolbox in Simulink. *Energy and Buildings*, 39(6):665–674, jun 2007. [4](#)

[35] G. H. Kanevce, L. P. Kanevce, G. S. Dulikravich, and H. R. B. Orlande. Estimation of thermophysical properties of moist materials under different drying conditions. *Inverse Problems in Science and Engineering*, 13(4):341–353, aug 2005. [6](#)

[36] M. Karalashvili, W. Marquardt, and A. Mhamdi. Optimal experimental design for identification of transport coefficient models in convection-diffusion equations. *Computers & Chemical Engineering*, 80:101–113, sep 2015. [11](#)

[37] I. V. Koptyug, S. I. Kabanikhin, K. T. Iskakov, V. B. Fenelonov, L. Y. Khitrina, R. Z. Sagdeev, and V. N. Parmon. A quantitative NMR imaging study of mass transport in porous solids during drying. *Chemical Engineering Science*, 55(9):1559–1571, may 2000. [26](#)

[38] J. Kwiatkowski, M. Woloszyn, and J.-J. Roux. Modelling of hysteresis influence on mass transfer in building materials. *Building and Environment*, 44(3):633–642, mar 2009. [13](#)

[39] A. V. Luikov. *Heat and mass transfer in capillary-porous bodies*. Pergamon Press, New York, 1966. [4](#), [7](#)

[40] N. Mendes, M. Chhay, J. Berger, and D. Dutykh. *Numerical methods for diffusion phenomena in building physics*. PUCPRes, Curitiba, Parana, 2017. [4](#), [5](#)

[41] N. Mendes and P. C. Philippi. Multitridiagonal-Matrix Algorithm for Coupled Heat Transfer in Porous Media: Stability Analysis and Computational Performance. *Journal of Porous Media*, 7(3):193–212, 2004. [5](#)

[42] N. Mendes and P. C. Philippi. A method for predicting heat and moisture transfer through multilayered walls based on temperature and moisture content gradients. *Int. J. Heat Mass Transfer*, 48(1):37–51, 2005. [4](#), [5](#)

[43] N. Mendes, I. Ridley, R. Lamberts, P. C. Philippi, and K. Budag. Umidus: A PC program for the Prediction of Heat and Mass Transfer in Porous Building Elements. In *IBPSA 99*, pages 277–283, Japan, 1999. International Conference on Building Performance Simulation. [4](#)

[44] A. Nassiopoulos and F. Bourquin. On-Site Building Walls Characterization. *Numerical Heat Transfer, Part A: Applications*, 63(3):179–200, jan 2013. [6](#)

[45] A. V. Nenarokomov and D. V. Titov. Optimal experiment design to estimate the radiative properties of materials. *Journal of Quantitative Spectroscopy and Radiative Transfer*, 93(1–3):313–323, jun 2005. [10](#)

[46] M. N. Ozisik and H. R. B. Orlande. *Inverse Heat Transfer: Fundamentals and Applications*. CRC Press, New York, 2000. [10](#)

[47] H. Rafidiarison, R. Rémond, and E. Mougel. Dataset for validating 1-D heat and mass transfer models within building walls with hygroscopic materials. *Building and Environment*, 89:356–368, jul 2015. [13](#)

[48] S. Rouchier, T. Busser, M. Pailha, A. Piot, and M. Woloszyn. Hygric characterization of wood fiber insulation under uncertainty with dynamic measurements and Markov Chain Monte-Carlo algorithm. *Building and Environment*, 114:129–139, mar 2017. [6](#)

[49] S. Rouchier, M. Woloszyn, G. Foray, and J.-J. Roux. Influence of concrete fracture on the rain infiltration and thermal performance of building facades. *Int. J. Heat Mass Transfer*,

61:340–352, jun 2013. 5

[50] S. Rouchier, M. Woloszyn, Y. Kedowide, and T. Béjat. Identification of the hygrothermal properties of a building envelope material by the covariance matrix adaptation evolution strategy. *J. Building Perf. Simul.*, 9(1):101–114, jan 2016. 6

[51] F. Tariku, K. Kumaran, and P. Fazio. Transient model for coupled heat, air and moisture transfer through multilayered porous media. *Int. J. Heat Mass Transfer*, 53(15-16):3035–3044, jul 2010. 7

[52] D. Ucinski. *Optimal Measurement Methods for Distributed Parameter System Identification*. 2004. 11

[53] A. Vande Wouwer, N. Point, S. Porteman, and M. Remy. An approach to the selection of optimal sensor locations in distributed parameter systems. *Journal of Process Control*, 10(4):291–300, aug 2000. 11

[54] M. Woloszyn and C. Rode. Tools for performance simulation of heat, air and moisture conditions of whole buildings. *Building Simulation*, 1(1):5–24, mar 2008. 4

[55] X. Xu and S. Wang. Optimal simplified thermal models of building envelope based on frequency domain regression using genetic algorithm. *Energy and Buildings*, 39(5):525–536, may 2007. 6

**J. BERGER:** LOCIE, UMR 5271 CNRS, UNIVERSITÉ SAVOIE MONT BLANC, CAMPUS SCIENTIFIQUE, F-73376 LE BOURGET-DU-LAC CEDEX, FRANCE

*E-mail address:* Berger.Julien@univ-smb.fr

*URL:* [https://www.researchgate.net/profile/Julien\\_Berger3/](https://www.researchgate.net/profile/Julien_Berger3/)

**T. BUSSER:** LOCIE, UMR 5271 CNRS, UNIVERSITÉ SAVOIE MONT BLANC, CAMPUS SCIENTIFIQUE, F-73376 LE BOURGET-DU-LAC CEDEX, FRANCE

*E-mail address:* Thomas.Busser@univ-smb.fr

*URL:* [https://www.researchgate.net/profile/Thomas\\_Busser/](https://www.researchgate.net/profile/Thomas_Busser/)

**D. DUTYKH:** LAMA, UMR 5127 CNRS, UNIVERSITÉ SAVOIE MONT BLANC, CAMPUS SCIENTIFIQUE, F-73376 LE BOURGET-DU-LAC CEDEX, FRANCE

*E-mail address:* Denys.Dutykh@univ-smb.fr

*URL:* <http://www.denys-dutykh.com/>

**N. MENDES:** THERMAL SYSTEMS LABORATORY, MECHANICAL ENGINEERING GRADUATE PROGRAM, PONTIFICAL CATHOLIC UNIVERSITY OF PARANÁ, RUA IMACULADA CONCEIÇÃO, 1155, CEP: 80215-901, CURITIBA – PARANÁ, BRAZIL

*E-mail address:* Nathan.Mendes@pucpr.edu.br

*URL:* [https://www.researchgate.net/profile/Nathan\\_Mendes/](https://www.researchgate.net/profile/Nathan_Mendes/)